European Journal of Geography

Volume 12, Issue 3, pp. 113 - 129

Article Info
Accepted: 11/11/2021
Corresponding Author: * florim.isufi@uni-pr.edu
DOI: https://doi.org/10.48088/ejg.a.ber.12.3.113.129

Research Article

Mapping summer SUHI and its impact on the environment using GIS and Remote Sensing techniques: A case study on Municipality of Prishtina (Kosovo)

Albert **Berila**[1] &
Florim **Isufi**[1*]

[1] *University of Prishtina, Kosovo*

Keywords

Summer SUHI,
LST,
GIS,
Remote Sensing,
Prishtina

Abstract

Urban areas, compared to peripheral and rural areas, have higher temperatures which are caused by a series of unplanned activities that are undertaken by humans. Such a thing leads to the emergence of the Surface Urban Heat Island (SUHI) phenomenon. In this paper, summer SUHI is determined through the calculation of LST for the Municipality of Prishtina using GIS and Remote Sensing techniques. To make this calculation, the Landsat 8 satellite image with 0% cloud cover was used. From the calculations made it turns out that the pixels with the highest value of LST are found in those parts where the urban area appears, where there are numerous constructions with impermeable materials, as well as in those areas where there are bare surfaces. Whereas, the pixels with lower values of LST appear in those parts where there are vegetation and water bodies, making these areas fresher. The SUHI phenomenon makes the lives of citizens difficult, therefore, such information is very important for the leaders and urban planners of the city of Prishtina, so that they take a series of steps towards minimizing such an effect in order to the life of the citizens to be as healthy as possible.

Highlights:

-Mapping Summer SUHI using GIS and Remote Sensing

-Make connectivity between the atmosphere and LST in order to identify the areas that face this undesirable phenomenon

-Presentation of the methodology for calculating LST in order to identify areas that face the SUHI phenomenon.

The publication of the European Journal of Geography (EJG) is based on the European Association of Geographers' goal to make European Geography a worldwide reference and standard. Thus, the scope of the EJG is to publish original and innovative papers that will substantially improve, in a theoretical, conceptual or empirical way the quality of research, learning, teaching and applying geography, as well as in promoting the significance of geography as a discipline. Submissions are encouraged to have a European dimension. The European Journal of Geography is a peer-reviewed open access journal and is published quarterly.

1. INTRODUCTION

Earth is the only planet on which life takes place. Throughout the organization of human life, natural elements have always played a very important role – depending on the degree of technological and human development. Among the most important/powerful ecological factors are humans – by constantly acting in the living environment have radically changed the living space and defining the paths of further development. But, with all these uncontrolled actions, human is making changes which are going to his detriment. These actions will have great consequences on the existence of the generations to come because are breaking the laws which are balanced and which exist millions of years ago.

In addition to the role of other natural sciences, a greater emphasis falls on the science of Geography. This science should give its contribution regarding the mapping and presentation of phenomena using conventional signs. This is done in order to illustrate the phenomena in different spaces – small or large. All this development, which is constantly following humanity, is seriously questioning the natural balance. It is here that geography (experts in this field) must intervene in all this disorder that has been made in the space around us, which, once, was almost free (unoccupied) and empty, while now overloaded and very dense with more and more inhabitants, construction and waste. At the moment, an approach to geography is more than necessary in the case of the extension and placement of industrial facilities, settlements, infrastructure, services, etc., in order to provide the most adequate solutions – sustainable development.

From all that has been said above about our living environment, it can be concluded quite clearly that humanity can no longer continue with such steps towards the future – neglect of the living environment – an integral part of human life. Any thoughtless behavior of the human factor towards the environment will turn into horrible events for him. Now more than ever it is necessary to avoid, as much as possible, the destruction of many components of the environment. The basic factor that determines the level of contemporary and economic civilization is the use of natural resources by human. Therefore, without a rational and controlled use of them, the future of humanity can not be imagined.

The great increase of the population has made the process of urbanization take a big boost of development. Such a process, if it took place incorrectly, the impact it will have on people and the environment around us will undoubtedly be negative. Therefore, such a process needs to be developed positively (Morefield et al., 2018; Berila & Isufi, 2021). If we analyze such a large development and at such a fast pace, we will notice that the effects, of course, will not be satisfactory. From such processes occur effects which are considered as harmful and which are: the increase of built-up areas; expansion of impermeable surfaces; reduction of natural surfaces; damage to forest areas, etc. Such cases, in abundance, we encounter in cities. These are exactly the reasons why in cities the temperature is higher than its periphery. Such changes have led to the emergence of a phenomenon called UHI (Urban Heat Island). UHI is a phenomenon in which temperatures in urban areas are higher compared to their suburbs or rural areas (Wang et al., 2017). As we are aware, there is a constant increase in the number of population in urban areas. Such an increase means an increase in all human activities, which, unfortunately, reinforce the UHI phenomenon. Therefore, it can be rightly said that this phenomenon is seriously threatening humans – especially those living in cities (Mohajerani et al., 2017) and that there will be many consequences in many sectors of life – air pollution, human health, energy management, etc. (Peres et al., 2018; Vintar Mally, 2021). It is precisely human activities that cause the UHI phenomenon to occur. This happens when the soil cover is transformed – natural surfaces become impermeable (concrete, asphalt, low albedo materials) (Buyantuyev & Wu, 2009; EPA, 2017; Harlan & Ruddell, 2011; Mavrogianni et al., 2011; Santamouris et al., 2011). It should be a top priority for city managers and urban planners to minimize such a harmful phenomenon as much as possible. It remains a task to find a way to prevent such a phenomenon – at best.

The UHI phenomenon has its types – depending on how the temperature is measured (Fabrizi et al., 2010; Sherafati et al., 2018):

a) CLHI (Canopy Layer Heat Island) – this layer lies approximately at the average height of buildings and is determined by measuring the air temperature at a height of 2 meters above the ground. The CLHI has usually measured through sensors mounted on fixed meteorological stations (Clay et al., 2006; Nichol et al., 2009; Schwarz et al., 2012; Smoliak et al., 2015).

b) Boundary Layer Heat Island (BLHI) – lies above the CLHI layer and can reach a thickness of up to 1 km. It is measured using special platforms, such as radiosondes and aircraft (Sherafati et al., 2018; Voogt, 2008).

c) SUHI (Surface Urban Heat Island) – difference in radiant temperature between urban and non-urban surfaces. The measurement/determination of this layer is done using thermal remote sensors (Voogt & Oke, 2003).

Various ways of measuring the UHI phenomenon have been presented in the scientific literature. Which way the researcher chooses, depends entirely on the availability of equipment/data and the accuracy required (Schwarz et al., 2012). Measuring the UHI phenomenon using geospatial technology represents SUHI (Surface Urban Heat Island) (Zhou et al., 2018). This is evident in cases where the study area has insufficient data on the measured temperature – the distribution of measuring equipment is inhomogeneous and rare. Thus, the use of geospatial technology emerges as a suitable tool to determine such a phenomenon through the calculation of LST (Land Surface Temperature) (Pour & Voženílek, 2020; Despini et al., 2016; Voogt & Oke, 2003). Atmospheric UHI is called as such by merging BLHI and CLHI. If we make the comparison between SUHI and atmospheric UHIs then it turns out that SUHI has a higher value during the day (Roth et al., 1989; Yuan & Bauer, 2007). Consequently, it falls to SUHI that it will be of higher value during the summer season when the sunlight falls at a more right angle and the conditions are generally drier (Oke, 1987). For all the factors we are talking about, which cause the appearance of the SUHI phenomenon, it is clear that the countries that will be at war with it are those countries that are developing – the most vulnerable/attacked (Mubea et al., 2011; Lee & Chang, 2011; Kityuttachai et al., 2013; Berila & Isufi, 2021; Sudhira et al., 2003; Kamusoko & Aniya, 2007; Kamusoko & Aniya, 2009; Liu et al., 2011; Moghadam & Helbich, 2013). Kosovo has not escaped this development, which also brings negative effects and the appearance of dangerous phenomena. Major challenges arise in the capital of Kosovo – Prishtina. All this happens due to the extraordinary changes that this city has experienced.

The purpose of our work is to map the summer SUHI for the entire Municipality of Prishtina and to make connectivity between the atmosphere and LST in order to identify the areas that face this undesirable phenomenon and to see if the areas with the greatest impact of this phenomenon are exactly those in it which human activities are most pronounced. The identification of these areas will be of great importance because it will enable the city managers to take the necessary mitigations in those places where the population faces this phenomenon.

2. STUDY AREA

Prishtina, taking into account its geographical location, occupies a suitable geographical position because it has a central location in the Balkan Peninsula (Figure 1). Whereas, within the Republic of Kosovo, this city occupies the northeastern part. Prishtina is surrounded by the following municipalities: Kastriot (Obiliq) in the west, Podujeva in the north, Graçanicë and Lipjan in the south, Fushë Kosova in the southwest, Kamenica in the east, Novobërdë in the southeast. Whereas, with the Republic of Serbia it borders on the northeastern part (Isufi & Berila, 2021) (Figure 2).

Figure 1. Location of the study area.

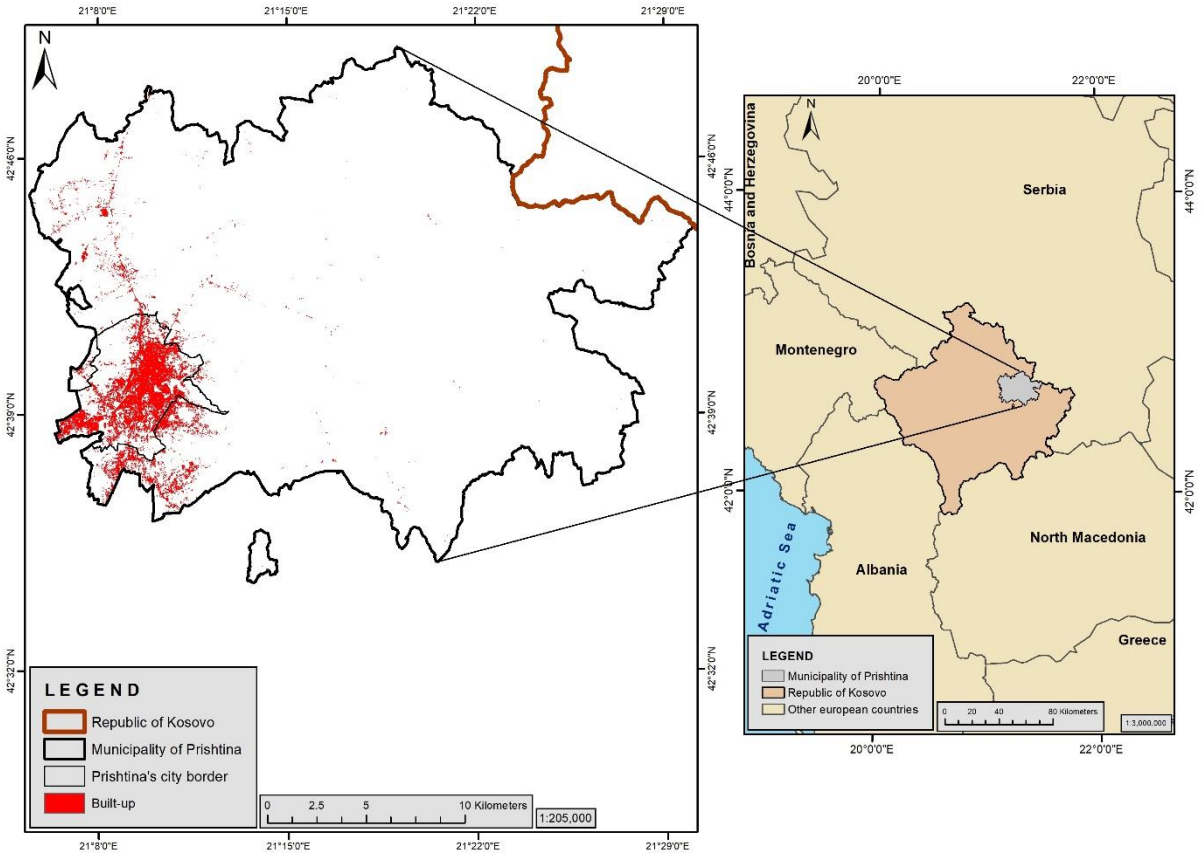

The whole municipality occupies approximately 523 km^2. It lies in the morphological plan of Kosovo and represents an alluvial plan covered with sediments of lakes, and geologically it is a tectonic depression, which has risen long Oligo-Miocene changes (Municipality of Prishtina, 2013; Isufi & Berila, 2021). The climate of our study area is continental with hot summers, cold winters, with 600 mm of rainfall on average per year (Municipality of Prishtina, 2013; Isufi & Berila, 2021). Our study area has hilly-mountainous relief in the southeastern, northeastern, and eastern parts. Somewhere, approximately, 535-580 meters goes the altitude of the western part and, if we exclude the eastern part, for the slope of the terrain we can say that it is low (Municipality of Prishtina, 2013; Berila & Isufi, 2021).

Prishtina, in Kosovo, is the largest cultural, administrative and economic center. It has a total population of 216,870 (KAS, 2020). In Prishtina, the change that has undergone in many parts of it is clearly noticeable. These changes, unfortunately, are for the most part negative – unplanned constructions, occupation of agricultural land with impermeable areas, a large expansion of the urban area (Isufi & Berila, 2021), etc. The increase of the population that Prishtina has experienced, and all other socio-economic developments, has made the needs increase. Consequences of all this are the great increase in population density, the increase of illegal constructions, the increase of unplanned constructions, etc. (Berila & Isufi, 2021; Isufi & Berila, 2021).

Figure 2. Satellite image of Prishtina – Landsat 8.

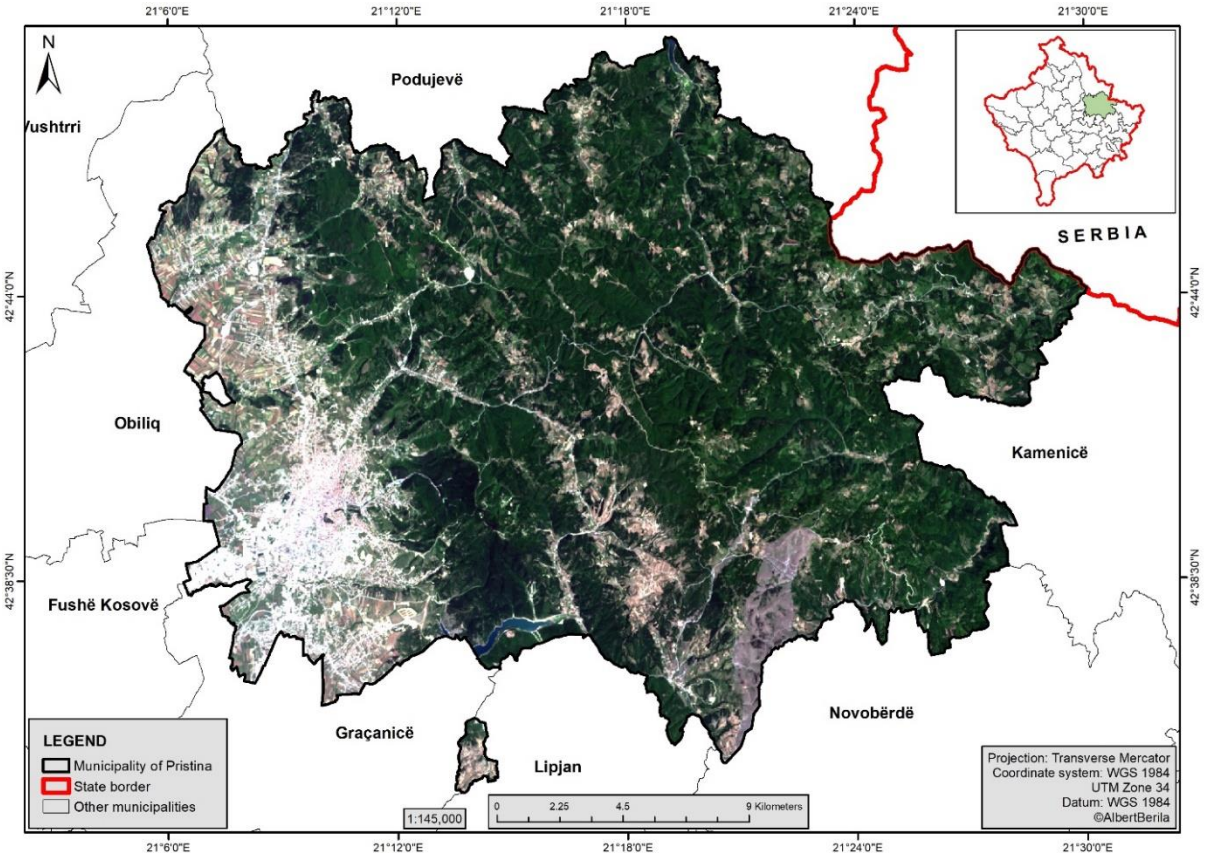

It is impossible not to mention that all this chaotic situation has been contributed also by the political aspect – political interference/corruption (Berila & Isufi, 2021; Isufi & Berila, 2021). In Prishtina, as well as around the world, there have been population movements (migrations). These movements, towards Prishtina, have occurred especially from rural areas to urban ones. Such movements have caused radical changes in almost all spheres of life (Isufi & Berila, 2021; KAS, 2014). All the developments/changes that have taken place in Prishtina, have made today, the capital, face many challenges and problems. These problems make the lives of citizens more difficult – heavy vehicle traffic, increase in the density of buildings, increase in the density of residents, increase in pollution, etc. When the UHI phenomenon is added to all this, then the situation only gets worse. From what was said above, comes the importance of mapping this phenomenon for Prishtina, so that when identifying areas facing high values of this phenomenon, mitigations are taken to facilitate the lives of citizens.

3. DATA AND METHODS

To do the summer SUHI mapping, it is necessary to do the LST calculation. To do this, we used the Landsat 8 satellite image for July 2, 2019. We downloaded this image from the United States Geological Survey (USGS) – from Collection 1 and at a Level 1 and, thankfully, it was without any cloud cover (0%) (Table 1). The selection of this date of the Landsat 8 satellite image, which belongs to the summer season and that is not covered by clouds, was done on purpose because as we know, the SUHI phenomenon intensifies during the warm season and when the climatic conditions are drier. As mentioned above, the SUHI phenomenon becomes more severe and strikes more during the summer season – when the sunlight falls at a greater angle and when the numerous activities of the population (vehicles, industrial, commercial, etc.) are more pronounced. All these human activities cause a large

number of pollutants to be released into the atmosphere. In such a state, sunlight falls on the surface of the earth but, due to the greenhouse effect created, this long-wave radiation is not allowed to escape. Therefore, here is the moment when the SUHI phenomenon strikes causing many problems to the entire population living in that area.

Table 1. Characteristics of the satellite image used in this study

Sensor type	Date	Path/Row	Cloud cover	Spatial resolution	Format	Source
Landsat 8 OLI/TIRS	2019/07/02	185/30	0%	30 m	Tiff	https://earthexplorer.usgs.gov/

In calculating the LST, it is necessary to make some preliminary adjustments to the image – atmospheric correction (Berila and Isufi, 2021). We made this adjustment using the ENVI software through the DOS (Dark Object Subtraction) method. DOS is an effective and simple method which is used to make atmospheric correction for satellite images. This method assumes that an important component of atmospheric scattering is the reflection that occurs from dark objects. This method works by searching through each band to find the darkest pixel values. The value found is deducted. In this way the scattering is removed.

It is important to note that the Landsat Database has shown considerable benefit in relation to environmental and climate issues (Mfondum et al., 2016; Adeyeri et al., 2017; Alavipanah et al., 2010; Narayan et al., 2016). In our case, the goal was to make a connection between the atmosphere and the LST. This is because, as mentioned earlier, the highest SUHI values are reached during the summer season, when the climatic conditions are drier, and when the sunlight falls perpendicularly. In relation to this issue, LST has been shown to be a key element in achieving this connectivity (Sobrino et al., 2004b; Sobrino et al., 2003; Sobrino et al., 2004a; Adeyeri et al., 2017; Dickinson, 1983).

In maps, it is important to pay as much attention as possible to the presentation of the particular phenomenon. For such a thing, in order to have a better and more accurate picture of the presentation of the SUHI phenomenon, we have used High Resolution (HR) ALOS-PALSAR (Advanced Land Observing Satellite-Phased Array-Type L-band Synthetic Aperture Radar) RTC (Radiometrically Terrain Corrected) elevation model (DEM), as an auxiliary data source with a 12.5 m spatial resolution. We have downloaded this digital relief model from the Alaska Satellite Facility website (https://asf.alaska.edu/).

The Landsat 8 satellite was successfully launched on 11 February 2013 and deployed into orbit with two instruments onboard (Valizadeh Kamran et al., 2015): the Operational Land Imager (OLI) and the Thermal Infrared Sensor (TIRS), which jointly produce a multispectral image consisting of 11 spectral bands. OLI collects nine spectral bands including a pan band: bands 1-4 correspond to the visible part of the electromagnetic spectrum, bands 5-7 and 9 to near-infrared and shortwave infrared regions of the spectrum (Taloor et al., 2021) (all of these have a spatial resolution of 30 m) (Jeevalakshmi et al., 2017); band 8 is panchromatic, taking images in the wide visible wavelength range (0,503-0,676 μm) with 15 m spatial resolution. These bands allow obtaining various kinds of information on the characteristics of the land surface, including vegetation cover. Two spectral bands for infrared wavelength are collected by the TIRS instrument (Kesikoğlu et al., 2020). In previous sensors (TM and ETM +), these were covered by a single band: band 10 (TIRS 1, 10.6-11.19 μm) and band 11 (TIRS 2, 11.5-12.51 μm), both with 100 m spatial resolution (Table 2) (NASA, 2018).

In this paper, we have presented and explained in detail the entire methodology used to arrive at the mapping of the SUHI phenomenon – the compilation of the LST map. To have a clearer picture, we have prepared the diagram (Figure 3) which shows all the steps taken. However, the presentation and calculation in detail of each step will be presented in the following sections.

In Landsat 8 sensor satellite images, thermal data is stored in the form of digital numbers (DN). These numbers represent cells (pixels) that have not yet been calibrated into units (Käfer et al., 2020) that make sense (meaningful units). After taking satellite images, the first process or task is to return the digital numbers to radiance. The following equation was used to convert DNs to spectral radiance (USGS, 2019) in the Landsat 8 TIRS sensor (Isaya Ndossi et al., 2016; Mejbel Salih et al., 2018; Guha & Govil, 2020; Berila & Isufi, 2021):

$$L_\lambda = M_L \times Q_{cal} + A_L \quad (1)$$

where:
L_λ is TOA spectral radiance $(Watss/(m^2 \times srad \times \mu m))$, M_L is Band-specific multiplicative rescaling factor from the metadata, Q_{cal} is Quantized and calibrated standard product pixel values (DN), A_L is Band-specific additive rescaling factor from the metadata (Isaya Ndossi et al., 2016; Mejbel Salih et al., 2018; Guha & Govil, 2020; Berila & Isufi, 2021). The metadata of the satellite image is presented in Table 3 (Jeevalakshmi et al., 2017).

Table 2. OLI and TIRS – Landsat 8 spectral bands

Spectral Band	**Wavelength (μm)**	**Spatial Resolution (m)**
Band 1 – Coastal/Aerosol	0.435-0.451	30
Band 2 – Blue	0.452-0.512	30
Band 3 – Green	0.533-0.590	30
Band 4 – Red	0.636-0.673	30
Band 5 – NIR	0.851-0.879	30
Band 6 – SWIR 1	1.566-1.651	30
Band 7 – SWIR 2	2.107-2.294	30
Band 8 – Panchromatic	0.503-0.676	15
Band 9 – Cirrus	1.363-1.384	30
Band 10 – TIRS 1	10.60-11.19	100
Band 11 – TIRS 2	11.50-12.51	100

Table 3. Metadata of the satellite image

Band	**Variable**	**Description**	**Value**
10		Thermal band	
	K_1	Thermal constant	774.8853
	K_2		1321.0789
	M_L	Band-specific multiplicative rescaling factor	3.3420E-04
	A_L	Band-specific additive rescaling factor	0.10000

Figure 3. Flowchart depicting methodology

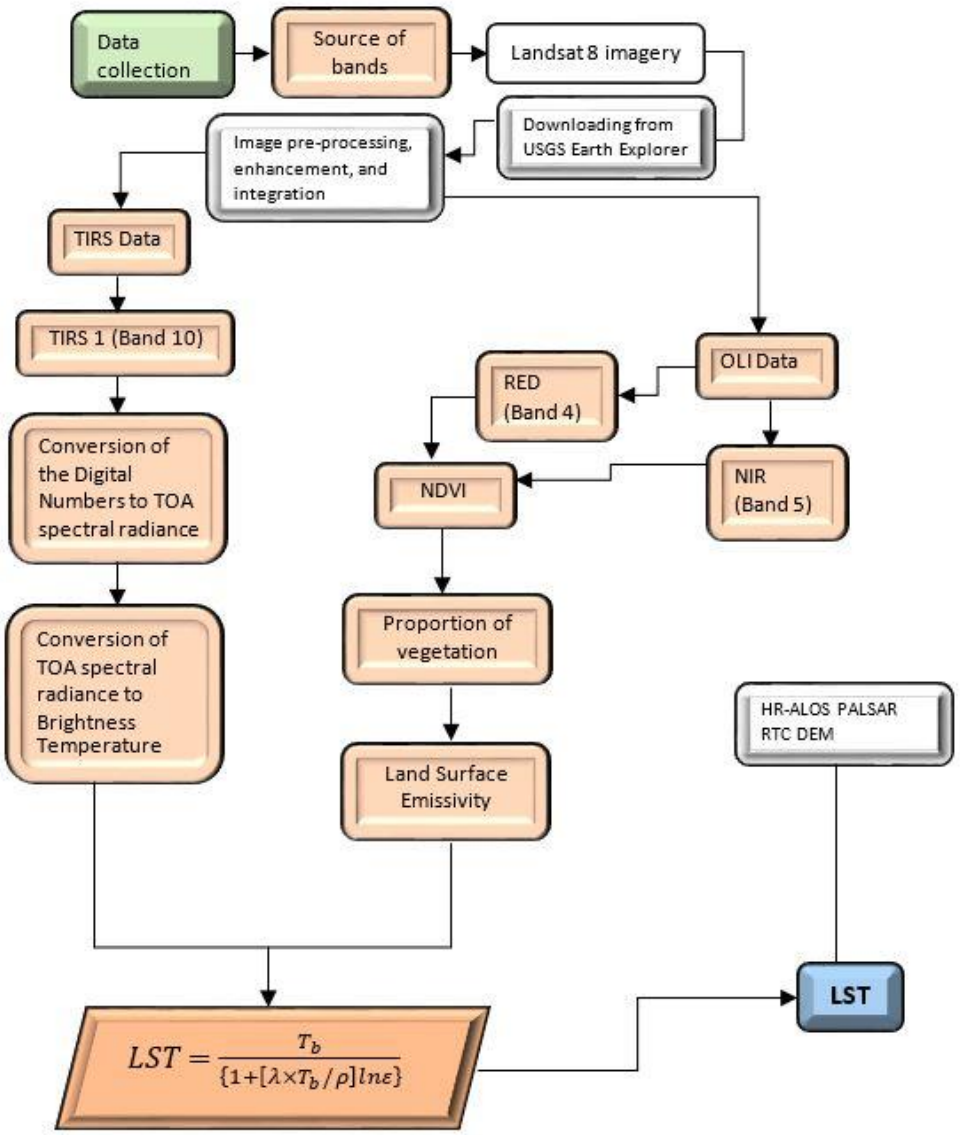

Then, in the Landsat 8 satellite image MTL file, the reflectance rescaling coefficients were obtained. This was done in order to transform the OLI band into TOA planetary reflection (Adeyeri et al., 2017). For such a thing, the following equation was used (Adeyeri et al., 2017):

$$\rho\lambda' = M_\rho Q_{cal} + A_\rho \quad (2)$$

Where:
$\rho\lambda'$ – TOA planetary reflectance, M_ρ – Band-specific multiplicative rescaling factor, A_ρ – Band-specific additive rescaling factor.
Making the correction of the TOA reflection with the angle of the sun, then is (USGS, 2019):

$$\rho\lambda = \frac{\rho\lambda'}{\cos(\theta_{sz})} = \frac{\rho\lambda'}{\sin(\theta_{se})} \quad (3)$$

Where:
$\rho\lambda'$ – TOA planetary reflectance; θ_{sz} – Local solar zenit angle, $\theta_{sz} = 90° - \theta_{se}$; θ_{se} – Local sun elevation angle (USGS, 2019).

The DOS (Dark Object Subtraction) method was used to remove small reflection values (due to air diffusion) (Chavez, 1996; Adeyeri et al., 2017). We used this method through the use of ENVI 5.3 software as we did not have at our disposal alternatives for atmospheric measurements (Adeyeri et al., 2017). The equation of an image corrected with DOS is (Adeyeri et al., 2017):

$$L_1P = L_1min - L_1(DO1\%) \quad (4)$$

Where:

L_1min – radiance corresponding to the minimum DN from the sum of all the pixels from the image, $L_1(DO1\%)$ – radiance of Dark Object assumed to have a reflectance of 0.01 (Adeyeri et al., 2017).

Although from the beginning of its operation TIRS has proven to be stable, still there were some elements (objects) that are hung in the image like errors in calibration and banding (Montanaro et al., 2014). Such a thing is caused by stray light effects. The impacts of these 2 effects are smaller in band 10 compared to band 11. Based on the numerous analyzes and studies that have been done, it has been concluded that band 10 of TIRS data is better and should be used instead of band 11. This, due to the good performance shown by band 10 (Adeyeri et al., 2017; Montanaro et al., 2014). For this study, TIRS band 10 was used.

3.1 Calculation of brightness temperature

The next step is to use the constant values given in the metadata in order to convert the spectral radiation to brightness temperature (T_b). In order to convert the radiance to brightness temperature, equation (5) has been used in the study (Isaya Ndossi et al., 2016; USGS, 2019):

$$T_b = \frac{K_2}{\ln\left[\frac{K_1}{L_\lambda}+1\right]} \quad (5)$$

Where:
T_b is the at-sensor brightness temperature [K], L_λ is the spectral radiance of thermal band 10 $[Wm^{-2}sr^{-1}\mu m^{-1}]$, K_1 is the band-specific thermal conversion constant from the metadata and K_2 band-specific thermal conversion constant from the metadata. The same equation is used for all sensors. The K_1 and K_2 values may vary depending on the sensor and the wavelengths by which the thermal bands operate (Isaya Ndossi et al., 2016; Yakar & Bilgi, 2019). The values of K_1 and K_2 can be obtained from the metadata file of the scene.

3.2 Estimation of land surface emissivity

To calculate the LST, it is necessary to evaluate the emissivity of the land surface (LSE) through the NDVI method (Jiménez-Muñoz et al., 2016; Valizadeh Kamran et al., 2015; Chakraborty et al., 2021). dε is the effect of the geometrical distribution of natural surfaces and internal reflections (Tan et al., 2010; Igun & Williams, 2018; Carrasco et al., 2020). To calculate the emissivity, we rely on the following equation (Guha & Govil, 2020):

$$d\varepsilon = (1-\varepsilon_s)(1-F_v)F_{\varepsilon_v} \quad (6)$$

Where:
ε_v is vegetation emissivity, ε_s is soil emissivity, F_v is fractional vegetation and F is a shape factor whose mean is 0.55 (Igun & Williams, 2018; Sobrino et al., 2004a; Guha & Govil, 2020).

$$\varepsilon = \varepsilon_v \times F_v + \varepsilon_s(1 - F_v) + d\varepsilon \quad (7)$$

Where:
ε is emissivity. From Equations (6) and (7), ε may be determined by the following equation (Yuvaraj, 2020):

$$\varepsilon = 0.004 \times F_v + 0.989 \quad (8)$$

The proportion of vegetation (F_v) is calculated based on the following equation (Wang et al., 2015; Yuvaraj, 2020):

$$\mathrm{F_v} = \left[\frac{\mathrm{NDVI} - \mathrm{NDVI_{min}}}{\mathrm{NDVI_{max}} - \mathrm{NDVI_{min}}}\right]^2 \quad (9)$$

The following equation is used to calculate NDVI with the help of Landsat visible (band 4) and NIR (band 5) images (Yuvaraj, 2020):

$$\mathrm{NDVI} = \frac{\mathrm{NIR-R}}{\mathrm{NIR+R}} = \frac{band\ 5 - band\ 4}{band\ 5 + band\ 4} \quad (10)$$

Where:
NIR and RED are the near-infrared and red band pixel values respectively (Alemu, 2019). The value of NDVI ranges between -1.0 and 1.0 (Alemu, 2019; Yuvaraj, 2020). High NDVI values indicate healthy vegetation while low values indicate less or no vegetation.

3.3 Calculation of LST

The final step of estimating the LST is as follows (Yuvaraj, 2020; Alemu, 2019; Weng et al., 2004):

$$LST = \frac{T_b}{\{1 + [\lambda \times T_b/\rho] ln\varepsilon\}} \quad (11)$$

Where:
λ is the wavelength of emitted radiance by Landsat 8 which is 10.8 (given by NASA), ε is the land surface emissivity, and ρ is given by the following equation (Yuvaraj, 2020):

$$\rho = h\frac{c}{\sigma} = 14388\ \mu m\ K \quad (12)$$

Where:
h is Planck's constant (6.626×10^{-34} Js), σ is the Boltzmann constant (1.38×10^{-23} J/K), and c is the velocity of light (2.988×10^{8} m/s) (Alemu, 2019; Yuvaraj, 2020).

4. RESULTS AND DISCUSSION

The importance of the natural soil cover, namely the vegetation, is extraordinary. Such a thing can be easily noticed as soon as we enter an urban area. During the summer season, when temperatures are high, as soon as we enter urban areas there is difficulty in carrying out our daily activities. This comes from the impermeable materials which are most abundant in these areas. These materials, as they have small albedo values, have the ability to absorb heat causing the temperature to rise. Due to such increased heat, the most exposed are children, the elderly, and all those who have breathing problems and similar diseases. Whereas, the complete opposite occurs in those areas where vegetation and water bodies predominate.

These areas, even during the summer season, are fresh, full of greenery, and minimize the SUHI effect. People, in these areas, freely carry out all their activities.

According to our LST map, compiled for our study area, we have noticed that the highest LST values are concentrated in those areas where impermeable materials predominate, as well as in all those areas where there is a lack of vegetation. Such areas are bare surfaces. Whereas, the complete opposite occurs in areas where there are vegetation and water bodies. In these areas, we have noticed the pixels with the lowest LST values. This is best seen in Figure 4. Here, LST values range from 296,485 K (lowest value) to 317,848 K (highest value). The pixels with the lowest LST values are located mainly in the parts where vegetation and water are located. Whereas, the pixels with the highest LST values lie mainly in the urban area (western part), in the southern part, and in those areas where there is vegetation damage. In the south there are bare surfaces and, as such, the layer without vegetation heats up quickly and easily, strengthening the SUHI effect.

Figure 4. Spatial distribution of LST for Prishtina

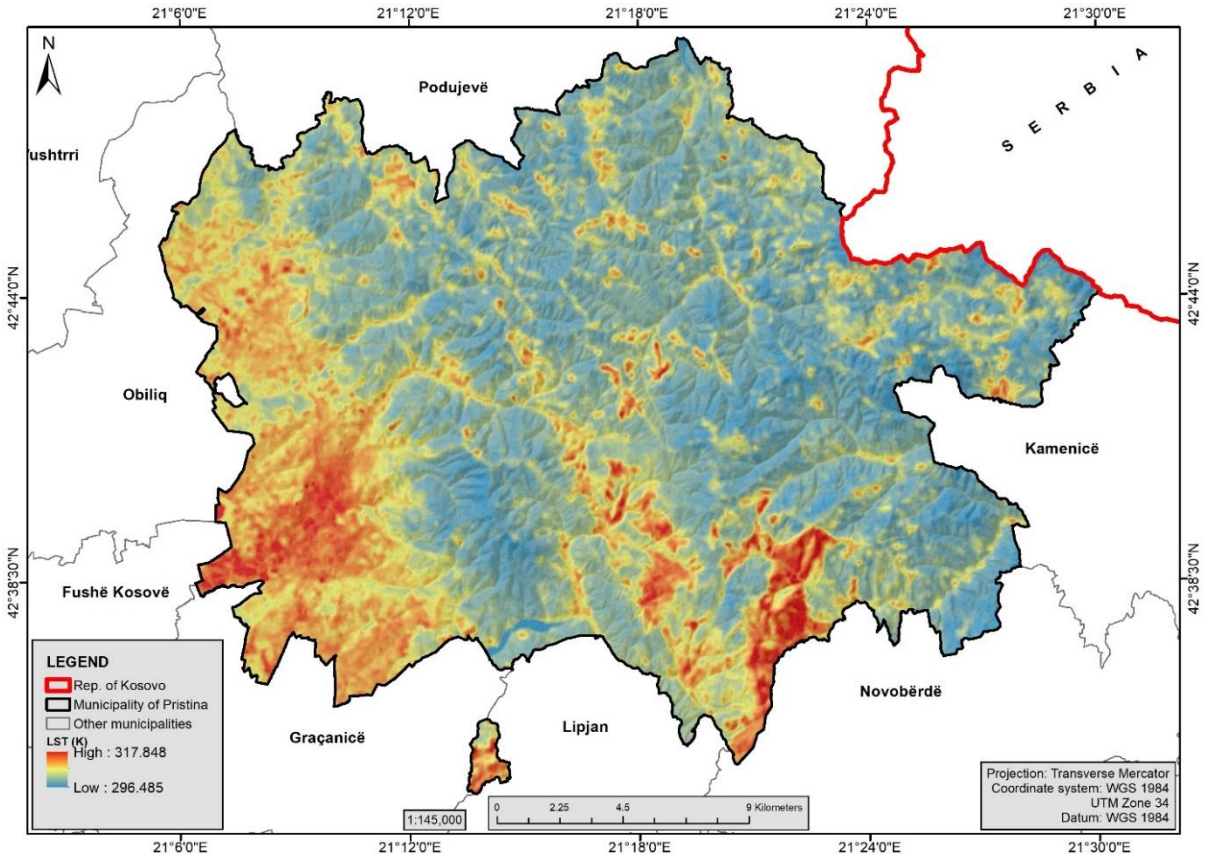

The connection between the development of human society and the development of settlements is inseparable. This is because, the more civilized a society is, the more extensive the settlements will be. But, unfortunately, human chose exactly the best and most suitable places for their construction, causing radical changes in the environment. In other words, the human with his uncontrolled activity constantly destroys and damages the natural cover, aggravating living conditions such as air, water, and land. The air in cities differs from the natural one because the amount of oxygen is reduced. While, on the other hand, the amount of harmful gases is high. The number of cities in the world is ever-increasing, and even cities with millions of inhabitants are constantly growing. Such growth is permanent, and the world is plunged into crisis. The rapid population growth in cities creates comprehensive problems. Wild constructions are becoming more and more of a problem. People, with the changes they

are making due to increased demand, are losing contact with the natural environment. Various pollutants that come from human activities, heavy traffic, industry, fossil fuels, etc., are reducing the process of photosynthesis and, consequently, are reducing the amount of oxygen. As a result of these processes, climatic conditions are being created which are different from the surroundings. It is necessary to control the development processes in these cities, otherwise, they will be plunged into urban chaos.

From the compilation of the LST map, we made a comparison between rural and urban areas. Regarding the values of LST, we found that the pixels with the highest value of LST are found exactly in urban spaces (317,848 K), while, on the other hand, the presence of green areas and water surfaces made the pixels with values lower (296,485 K) of LST to be distributed in rural areas.

Similar results as in our paper were observed in the work of Li et al. (2014). In this paper, the pixels with the highest LST values were distributed in both residential and industrial areas in which vegetated areas were scarce or nonexistent. The same results were found by Gang et al. (2019). They found that the intensity of the SUHI phenomenon is related to different types of land use. According to them, the greater the conversion of natural surfaces into artificial surfaces, the greater the intensity of the SUHI phenomenon and vice versa.

From all the above it follows that a very big challenge in the Municipality of Prishtina is the unplanned use of natural resources – causing pollution and degradation of the environment to increase. Unplanned use of land with natural cover and its covering with impermeable materials will result in very big consequences – any change and transformation of natural areas into artificial ones will affect that the situation with the SUHI phenomenon worsens even more.

5. CONCLUSIONS

Our study includes GIS and Remote Sensing techniques to measure the SUHI phenomenon during the summer season. Such a measurement was made using the free Landsat 8 satellite image provided by USGS. The Landsat 8 TIRS (10) band is considered to be the most appropriate and effective way to calculate LST.

Areas that most strongly face the SUHI phenomenon were identified through LST calculation. Pixels with high LST values were investigated in the western part, where the urban area stands out, as well as to a large extent in the southern part, exactly where there is a bare surface. Whereas, low LST pixels were investigated in all areas where vegetation and water bodies predominated. The problematic issue with the SUHI effect is an issue that requires great attention because of the concerns it causes to citizens. So it's not a simple matter. Countries around the world face this problem – some more, some less.

From what was discussed above, we conclude that the greener areas they are, the better. City leaders need to take a series of steps that will minimize the SUHI effect, such as creating green areas in the city, using as little material as possible that has low albedo values, using green roofs on buildings, and so on. All these actions make the life of citizens better, healthier and promote sustainable development.

The high level of development with which Prishtina is being characterized, such as the large increase of population density, rapid urban expansion, increased demands for energy, industrial activities, etc., will make the peripheral areas affected by changes by causing the green space to be reduced. Based on this, the authors expect that policymakers and urban planners of the city of Prishtina take this information seriously in order for all future activities to be planned.

ACKNOWLEDGEMENTS

The authors wish to acknowledge the United States Geological Survey (USGS) for the provision of data used for this study.

REFERENCES

Adeyeri, O. E., Akinsanola, A. A., & Ishola, K. A. (2017). Investigating surface urban heat island characteristics over Abuja, Nigeria: Relationship between land surface temperature and multiple vegetation indices. *Remote Sensing Applications: Society and Environment*, 7, 57-68. https://doi.org/10.1016/j.rsase.2017.06.005.

Alavipanah, S. K., Saradjian, M., Savaghebi, G. R., Komaki, C. B., Moghimi, E., KarimpurReyhan, M. (2010). Land surface temperature in the yardang region of Lut desert (Iran) based on field measurements and landsat thermal data. *Journal of Agricultural Science and Technology*, 9, 287-303.

Alemu, M. M. (2019). Analysis of Spatio-Temporal Land Surface Temperature and Normalized Difference Vegetation Index Changes in the Andassa Watershed, Blue Nile Basin, Ethiopia. *Journal of Resources and Ecology*, 10(1), 77. https://doi.org/10.5814/j.issn.1674-764x.2019.01.010.

Berila, A., Isufi, F. (2021). Two Decades (2000–2020) Measuring Urban Sprawl Using GIS, RS and Landscape Metrics: a Case Study of Municipality of Prishtina (Kosovo). *Journal of Ecological Engineering*, 22(6), 114-125. https://doi.org/10.12911/22998993/137078.

Buyantuyev, A., & Wu, J. (2009). Urban heat islands and landscape heterogeneity: linking spatiotemporal variations in surface temperatures to land-cover and socioeconomic patterns. *Landscape Ecology*, 25(1), 17-33. http://dx.doi.org/10.1007/s10980-009-9402-4.

Carrasco, R. A., Pinheiro, M. M. F., Junior, J. M., Cicerelli, R. E., Silva, P. A., Osco, L. P., & Ramos, A. P. M. (2020). Land use/land cover change dynamics and their effects on land surface temperature in the western region of the state of São Paulo, Brazil. *Regional Environmental Change*, 20(3). https://doi.org/10.1007/s10113-020-01664-z.

Chakraborty, T., Lee, X., Ermida, S., & Zhan, W. (2021). On the Land Emissivity Assumption and Landsat-Derived Surface Urban Heat Islands: A Global Analysis. *Remote Sensing of Environment*, 265. https://doi.org/10.1016/j.rse.2021.112682.

Chavez, P.S. (1996). Image-Based Atmospheric Corrections – Revisited and Improved. *Photogrammetric Engineering and Remote Sensing*, 62(9), 1025-1036.

Clay, R., Guan, H., Wild, N., Bennett, J., Vinodkumar, & Ewenz, C. (2016). Urban Heat Island traverses in the City of Adelaide, South Australia. *Urban Climate*, 17, 89-101. http://dx.doi.org/10.1016/j.uclim.2016.06.001.

Despini, F., Ferrari, C., Bigi, A., Libbra, A., Teggi, S., Muscio, A., & Ghermandi, G. (2016). Correlation between remote sensing data and ground based measurements for solar reflectance retrieving. *Energy and Buildings*, 114, 227-233. http://dx.doi.org/10.1016/j.enbuild.2015.06.018.

Dickinson, R. E. (1983). Land Surface Processes and Climate – Surface Albedos and Energy Balance. Theory of Climate, *Proceedings of a Symposium Commemorating the Two-Hundredth Anniversary of the Academy of Sciences of Lisbon*, 305-353. http://dx.doi.org/10.1016/s0065-2687(08)60176-4.

Environmental Protection Agency (EPA). (2017). *Reducing Urban Heat Islands: Compendium of Strategies*; US Environmental Protection Agency: Washington, DC, USA.https://www.epa.gov/sites/production/files/2014-06/documents/basicscompendium.pdf. (Accessed 2021-04-25).

Fabrizi, R., Bonafoni, S., & Biondi, R. (2010). Satellite and Ground-Based Sensors for the Urban Heat Island Analysis in the City of Rome. *Remote Sensing*, 2(5), 1400-1415. http://dx.doi.org/10.3390/rs20514.

Gang, W., QiuPing, Zh., RongBo. X., & DongSheng, G. (2019). On impacts of land use, population density and altitude on the urban heat island. *Journal of Yunnan University - Natural Sciences Edition*, 41(1), 82-90. https://doi.org/10.7540/j.ynu.20170584.

Guha, S., & Govil, H. (2020). Land surface temperature and normalized difference vegetation index relationship: a seasonal study on a tropical city. *SN Applied Sciences*, 2(10). https://doi.org/10.1007/s42452-020-03458-8.

Harlan, S. L., & Ruddell, D. M. (2011). Climate change and health in cities: impacts of heat and air pollution and potential co-benefits from mitigation and adaptation. *Current Opinion in Environmental Sustainability*, 3(3), 126-134. http://dx.doi.org/10.1016/j.cosust.2011.01.001.

Igun, E., & Williams, M. (2018). Impact of urban land cover change on land surface temperature. *Global Journal of Environmental Science and Management*, 4, 47-58. https://doi.org/10.22034/gjesm.2018.04.01.005.

Isaya Ndossi, M., & Avdan, U. (2016). Application of Open Source Coding Technologies in the Production of Land Surface Temperature (LST) Maps from Landsat: A PyQGIS Plugin. *Remote Sensing*, 8(5), 413. https://doi.org/10.3390/rs8050413.

Isufi, F., Berila, A. (2021). Using geospatial technology to analyse land use/cover changes in Prishtina, Kosovo (2000–2020). *GeoJournal*. https://doi.org/10.1007/s10708-021-10452-z.

Jeevalakshmi, D., Narayana Reddy, S., Balakrishnan Manikiam, B. (2017). Land surface temperature retrieval from LANDSAT data using emissivity estimation. *International Journal of Applied Engineering Research*, 12(20), 9679-9687.

Jiménez-Muñoz, J. C., Sobrino, J. A., Gillespie, A., Sabol, D., & Gustafson, W. T. (2006). Improved land surface emissivities over agricultural areas using ASTER NDVI. *Remote Sensing of Environment*, 103(4), 474-487. http://dx.doi.org/10.1016/j.rse.2006.04.012.

Käfer, P. S., Rolim, S. B. A., Diaz, L. R., Rocha, N. S. da, Iglesias, M. L., & Rex, F. E. (2020). Comparative analysis of split-window and single-channel algorithms for land surface temperature retrieval of a pseudo-invariant target. *Boletim de Ciências Geodésicas*, 26(2). https://doi.org/10.1590/s1982-21702020000200008.

Kamusoko, C., & Aniya, M. (2007). Land use/cover change and landscape fragmentation analysis in the Bindura District, Zimbabwe. *Land Degradation & Development*, 18(2), 221-233. https://doi.org/10.1002/ldr.761.

Kamusoko, C., Aniya, M. (2009). Hybrid classification of Landsat data and GIS for land use/cover change analysis of the Bindura district, Zimbabwe. International *Journal of Remote Sensing*, 30(1), 97-115. https://doi.org/10.1080/01431160802244268.

KAS (Kosovo Agency of Statistics). (2014). *Kosovan Migration, Prishtina*. https://ask.rks-gov.net/media/1380/kosovan-migration-2014.pdf. (Accessed 2021-03-27).

KAS (Kosovo Agency of Statistics). (2020). *Statistical yearbook of the Republic of Kosovo, Prishtina*. https://ask.rks-gov.net/media/5629/vjetari-final-2020-per-web.pdf. (Accessed 2021-04-03).

Kesikoğlu, M., Çiçekli, S. Y., & Kaynak, T. (2020). The identification of coastline changes from landsat 8 satellite data using artificial neural networks and k-nearest neighbor. *Turkish Journal of Engineering*, 4(1), 47-56. https://doi.org/10.31127/tuje.599359.

Kityuttachai, K., Tripathi, N.K., Tipdecho, T., & Shrestha, R. (2013). CA-Markov analysis of constrained coastal urban growth modeling: Hua Hin seaside city, Thailand. *Sustainability*, 5(4), 1480–1500. https://doi.org/10.3390/su5041480.

Lee, Y., & Chang, H. (2011). The simulation of land use change by using CA-Markov model: a case study of Tainan City, Taiwan. *19th International Conference on Geoinformatics*, 24-26 June, 1-4. https://doi.org/10.1109/geoinformatics.2011.5980819.

Li, L., Tan, Y., Ying, S., Yu, Z., Li, Z., & Lan, H. (2014). Impact of land cover and population density on land surface temperature: case study in Wuhan, China. *Journal of Applied Remote Sensing*, 8(1), 084993. https://doi.org/10.1117/1.jrs.8.084993.

Liu, Y., Hou, S., Kong, X. & Xu, Y. (2011). The analysis on land use change in urban fringe area based on the GIS technology. *International Conference on Remote Sensing, Environment and Transportation Engineering*, 6444-6447. https://doi.org/10.1109/rsete.2011.5965832.

Mavrogianni, A., Davies, M., Batty, M., Belcher, S., Bohnenstengel, S., Carruthers, D., Chalabi, Z., Croxford, B., Demanuele, C., Evans, S., Girldharan, R., Hacker, J., Hamilton, I., Hogg, C., Hunt, J., Kolokotroni, M., Martin, C., Milner, J., Rajapaksha, I., … Ye, Z. (2011). The comfort, energy and health implications of London's urban heat island. *Building Services Engineering Research and Technology*, 32(1), 35-52. http://dx.doi.org/10.1177/0143624410394530.

Mejbel Salih, M., Zakariya Jasim, O., I. Hassoon, K., & Jameel Abdalkadhum, A. (2018). Land Surface Temperature Retrieval from LANDSAT-8 Thermal Infrared Sensor Data and Validation with Infrared Thermometer Camera. International *Journal of Engineering & Technology*, 7(4.20), 608. https://doi.org/10.14419/ijet.v7i4.20.27402.

Moghadam, H. H., & Helbich, M. (2013). Spatiotemporal urbanization processes in the megacity of Mumbai, India: a Markov chains-cellular automata urban growth model. *Applied Geography*, 40, 140-149. https://doi.org/10.1016/j.apgeog.2013.01.009.

Mohajerani, A., Bakaric, J., & Jeffrey-Bailey, T. (2017). The urban heat island effect, its causes, and mitigation, with reference to the thermal properties of asphalt concrete. *Journal of Environmental Management*, 197, 522-538. http://dx.doi.org/10.1016/j.jenvman.2017.03.095.

Montanaro, M., Gerace, A., Lunsford, A., & Reuter, D. (2014). Stray Light Artifacts in Imagery from the Landsat 8 Thermal Infrared Sensor. *Remote Sensing*, 6(11), 10435-10456. http://dx.doi.org/10.3390/rs61110435.

Morefield, P., Fann, N., Grambsch, A., Raich, W., & Weaver, C. (2018). Heat-Related Health Impacts under Scenarios of Climate and Population Change. *International Journal of Environmental Research and Public Health*, 15(11), 2438. http://dx.doi.org/10.3390/ijerph15112438.

Mubea, K., Ngigi, T., & Mundia, C. (2011). Assessing Application of Markov Chain Analysis in Nakuru. *Applied Geoinformatics for Society and Environment*, 182-188.

Municipality of Prishtina. (2013). *Municipal Development Plan of Prishtina 2012–2022*. https://prishtinaonline.com/uploads/prishtina_pzhk_2012-2022_shqip%20(1).pdf. (Accessed 2021-02-20).

Narayan, K., Khanindra, P., Abhisek, C., & Sahoo, S. (2016). Urban heat island explored by corelationship between land surface temperature vs multiplevegetation indices. *Spatial Information Research*, 24, 515-529. http://dx.doi.org/10.1007/s41324-016-0049-3.

NASA. (2018). *Landsat Science: Landsat 8 Overview*. https://landsat.gsfc.nasa.gov/landsat-8/landsat-8-overview/. (Accessed 2021-04-10).

Ngandam Mfondoum, A. H., Etouna, J., Nongsi, B. K., Mvogo Moto, F. A., … Noulaquape Deussieu, F. G. (2016). Assessment of Land Degradation Status and Its Impact in Arid and Semi-Arid Areas by Correlating Spectral and Principal Component Analysis Neo-Bands. *International Journal of Advanced Remote Sensing and GIS*, 5(1), 1539–1560. https://doi.org/10.23953/cloud.ijarsg.77.

Nichol, J. E., Fung, W. Y., Lam, K., & Wong, M. S. (2009). Urban heat island diagnosis using ASTER satellite images and "in situ" air temperature. *Atmospheric Research*, 94(2), 276-284. http://dx.doi.org/10.1016/j.atmosres.2009.06.011.

Oke, T. R. (1987). *Boundary layer climates*. London, Routledge.

Peres, L. F., Lucena, A. J., Rotunno Filho, O. C., & França, J. R. (2018). The urban heat island in Rio de Janeiro, Brazil, in the last 30 years using remote sensing data. *International Journal of Applied Earth Observation and Geoinformation*, 64, 104-116. http://dx.doi.org/10.1016/j.jag.2017.08.012.

Pour, T. & Voženílek, V. (2020). Thermal data analysis for urban climate research: A case study of Olomouc, Czechia. *Geographia Cassoviensis*, 14(1), 77-91. http://dx.doi.org/10.33542/gc2020-1-05.

Roth, M., Oke, T. R., & Emery, W. J. (1989). Satellite-derived urban heat islands from three coastal cities and the utilization of such data in urban climatology. *International Journal of Remote Sensing*, 10(11), 1699-1720. http://dx.doi.org/10.1080/01431168908904002.

Santamouris, M., Synnefa, A., & Karlessi, T. (2011). Using advanced cool materials in the urban built environment to mitigate heat islands and improve thermal comfort conditions. *Solar Energy*, 85(12), 3085-3102. http://dx.doi.org/10.1016/j.solener.2010.12.023.

Schwarz, N., Schlink, U., Franck, U., & Großmann, K. (2012). Relationship of land surface and air temperatures and its implications for quantifying urban heat island indi-cators – An application for the city of Leipzig (Germany). *Ecological Indicators*, 18, 693-704. http://dx.doi.org/10.1016/j.ecolind.2012.01.001.

Sherafati, S., Saradjian, M.R. & Rabbani, A. (2018). Assessment of Surface Urban Heat Island in Three Cities Surrounded by Different Types of Land-Cover Using Satellite Images. *Journal of the Indian Society of Remote Sensing*, 46, 1013-1022. https://doi.org/10.1007/s12524-017-0725-3.

Smoliak, B. V., Snyder, P. K., Twine, T. E., Mykleby, P. M., & Hertel, W. F. (2015). Dense Network Observations of the Twin Cities Canopy-Layer Urban Heat Island. *Journal of Applied Meteorology and Climatology*, 54(9), 899-1917. http://dx.doi.org/10.1175/jamc-d-14-0239.1.

Sobrino, J. A., Correspond, Jiménez-Muñoz, J. C., El-Kharraz, J., Gómez, M., Romaguera, M., & Sória, G. (2004b). Single-channel and two-channel methods for land surface temperature retrieval from DAIS data and its application to the Barrax site. *International Journal of Remote Sensing*, 25(1), 215-230. http://dx.doi.org/10.1080/0143116031000115210.

Sobrino, J. A., El-Kharraz, J., & Li, Z.-L. (2003). Surface temperature and water vapour retrieval from MODIS data. *International Journal of Remote Sensing*, 24(24), 5161-5182. http://dx.doi.org/10.1080/0143116031000102502.

Sobrino, J. A., Jiménez-Muñoz, J. C., & Paolini, L. (2004a). Land surface temperature retrieval from LANDSAT TM 5. *Remote Sensing of Environment*, 90(4), 434-440. http://dx.doi.org/10.1016/j.rse.2004.02.003.

Sudhira, H. S., Ramachandra, T. & Jagadish, K. (2003). Urban sprawl pattern recognition and modeling using GIS. *Map India Conference*, 28-31.

Taloor, A. K., Drinder Singh Manhas, & Chandra Kothyari, G. (2021). Retrieval of land surface temperature, normalized difference moisture index, normalized difference water index of the Ravi basin using Landsat data. *Applied Computing and Geosciences*, 9, 100051. https://doi.org/10.1016/j.acags.2020.100051.

Tan, K.C., Lim, H.S., MatJafri, M.Z., & Abdullah, K. (2010). Land Surface Temperature Retrieval by Using ATCOR3_T and Normalized Difference Vegetation Index Methods in Penang Island. *American Journal of Applied Sciences*, 7(5), 717–723. https://doi.org/10.3844/ajassp.2010.717.723.

USGS. (2019). *Using the USGS Landsat 8 Product*. https://prd-wret.s3.us-west-2.amazonaws.com/assets/palladium/production/atoms/files/LSDS-1574_L8_Data_Users_Handbook-v5.0.pdf. (Accessed 2021-02-10).

Valizadeh Kamran, K., Pirnazar, M., & Farhadi Bansouleh, V. (2015). Land surface temperature retrieval from Landsat 8 TIRS: comparison between split window algorithm and SEBAL method. *Third International Conference on Remote Sensing and Geoinformation of the Environment (RSCy2015)*. https://doi.org/10.1117/12.2192491.

Vintar Mally, K. (2021). Trends in regional development in Slovenia in the light of the goals of sustainable development. *European Journal of Geography*, 12(2), 36-51. https://doi.org/10.48088/ejg.k.mal.12.2.36.51

Voogt, J. (2008). How Researchers Measure Urban Heat Islands. https://19january2017snapshot.epa.gov/sites/production/files/2014-07/documents/epa_how_to_measure_a_uhi.pdf. (Accessed 2021-04-01).

Voogt, J. A., & Oke, T. R. (2003). Thermal remote sensing of urban climates. *Remote Sensing of Environment*, 86(3), 370-384. http://dx.doi.org/10.1016/s0034-4257(03)00079-8.

Wang, F., Qin, Z., Song, C., Tu, L., Karnieli, A., & Zhao, S. (2015). An Improved Mono-Window Algorithm for Land Surface Temperature Retrieval from Landsat 8 Thermal Infrared Sensor Data. *Remote Sensing*, 7(4), 4268-4289. http://dx.doi.org/10.3390/rs7.

Wang, H., Zhang, Y., Tsou, J., & Li, Y. (2017). Surface Urban Heat Island Analysis of Shanghai (China) Based on the Change of Land Use and Land Cover. *Sustainability*, 9(9), 1538. http://dx.doi.org/10.3390/su9091538.

Weng, Q., Lu, D., & Schubring, J. (2004). Estimation of land surface temperature–vegetation abundance relationship for urban heat island studies. *Remote Sensing of Environment*, 89(4), 467-483. http://dx.doi.org/10.1016/j.rse.2003.11.005.

Yakar, İ., & Bilgi, S. (2019). Land Surface Temperature mapping by the use of Remote Sensing and GIS: Case Study of Istanbul metropolitan area. *Conference: X. Türkiye Ulusal Fotogrametri ve Uzaktan Algılama Birliği Teknik Sempozyumu*.

Yuan, F., & Bauer, M. E. (2007). Comparison of impervious surface area and normalized difference vegetation index as indicators of surface urban heat island effects in Landsat imagery. *Remote Sensing of Environment*, 106(3), 375-386. https://doi.org/10.1016/j.rse.2006.09.003.

Yuvaraj, R. M. (2020). Extents of Predictors for Land Surface Temperature Using Multiple Regression Model. The Scientific World Journal, 2020, 1-10. https://doi.org/10.1155/2020/3958589.

Zhou, D., Xiao, J., Bonafoni, S., Berger, C., Deilami, K., Zhou, Y., … Sobrino, J. (2018). Satellite Remote Sensing of Surface Urban Heat Islands: Progress, Challenges, and Perspectives. *Remote Sensing*, 11(1), 48. https://doi.org/10.3390/rs11010048.